Journal of Materials Chemistry C

Accepted Manuscript

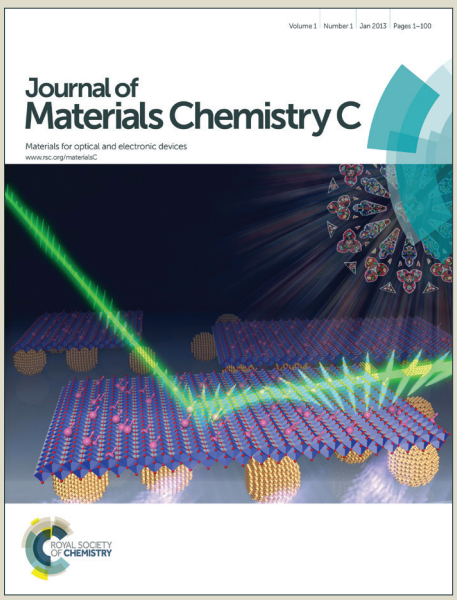

ROYAL SOCIETY OF CHEMISTRY

www.rsc.org/materialsC

Cite this: DOI: 10.1039/c0xx00000x

www.rsc.org/xxxxxx

ARTICLE TYPE

Enhancing the blue phosphorescence of iridium complexes with dicyclometalated phosphite ligand via aza-substitution: a density functional theory investigation

Gahungu Godefroid [a,b], Liu Yuqi [a], Si Yanling [a], Su Juanjuan [a], Qu Xiaochun [a], Shang Xiaohong [a] and Wu Zhijian [a]*

Received (in XXX, XXX) X[th] XXXXXXXXX 20XX, Accepted X[th] XXXXXXXXX 20XX
DOI: 10.1039/b000000x

Electronic structure methods based on judiciously chosen DFT and TD-DFT approaches were applied to explore the influence of the aza-substitution on the geometrical, electronic and photophysical properties of iridium complexes of dicyclometalated phosphite recently reported as good blue phosphorescents (*Angew. Chem. Int. Ed.*, 2011, **123**, 3240). With the respect to the pristine molecule, the frontier molecular orbitals (the HOMO & LUMO) were found to be stabilized upon the aza-substitution, with the magnitude of the decrease in orbital energy depending on the position of the substitution. The results also revealed a slightly enhanced LUMO-HOMO energy gap and consequently a deep blue shifted phosphorescence spectrum. In addition, the electron affinity, ionization potential, and charge mobility which are some other key factors in the design of optoelectronic materials, were found to be in general, improved by the aza-substitution considered in this study. Comparatively to the molecule parent, the aza-substituted counterparts show a well destabilized metal centered (^{3}MC d-d*) triplet and larger energy separation from the low-lying (^{3}MLCT π-π*) triplet, which is likely to enhance the reported phosphorescence efficiency. These features make the aza-substitution an efficient strategy to increase the ^{3}MLCT π-π* - ^{3}MC d-d* energy splitting without altering the blue emission of the kind of complexes under study.

Cite this: DOI: 10.1039/c0xx00000x

www.rsc.org/xxxxxx

ARTICLE TYPE

1. Introduction

Since the introduction of organometallic complexes as emitters in OLEDs, green and red spectral range phosphorescent OLEDs with high efficiency and stability have already been demonstrated.[1-3] However, there is still lack of stable and efficient blue-emitting OLEDs, which are essential for the commercial launch of such devices for lighting. Lots of effort has been done to shift the emission wavelength of organometallic complexes to the deep-blue spectral range, while maintaining a high radiative rate and high photoluminescence efficiency (Φ_{PL}). This is still a (particularly) challenging task since shifting the lowest emitting triplet state can lead to the population of non-radiative states. Indeed, designing new materials to show higher energy, such as deep-blue emission with an ideal CIE (Commission Internationale de l'Eclairage) coordinate encounters more obstacles than the progress made for obtaining green and red colors.

Considerable research has been invested in developing blue OLEDs with high external quantum efficiency as well as a deeper blue color. [4, 5]The first attempt was carried out by modifying the ligand structure of molecules with pyridine ligands. [6-8] However, it turned out that this approach is not suitable to reach efficient deep-blue emission because of a significant decrease in Φ_{PL} due to a close non-radiative state. The origin of the non-radiative state seems to lie on e_g orbitals, which promote non-luminescent d-d* transitions.[9,10] Although some achievements have been partly reported in terms of CIE_{xyz} coordinates, upon adoption of carbene-,[11] triazolyl-,[12] and fluorine-substituted bipyridine based chelates, [13] improvements to the efficiency and lifetime of blue OLEDs are still vital to the success of OLEDs as replacements for LCD technology, and organometallic complexes are to be designed in a way that the energy of such a non-radiative excited state is increased, inhibiting thermal population at room temperature. In a recent work, Lin et al. [14] reported on a new class of heteroleptic Ir (III) complexes incorporating tripodal, facially coordinated phosphate (or phosphonite denoted as P^C_2: see structures of **2a** and **3a** in scheme 1) ligand serving as the ancillary, together with the use of 2-(5-tert-butyl-2H-1,2,4-triazol-3-yl)pyridyl (*tbtp*) acting as blue chromophore. [15] Beside the good stabilization of complex and the necessary long-term stability in application, another advantage offered by the tridentate as P^C_2 chelate was reported to be its profound and versatile functionality, capable of fine-tuning the electronic character.[14] Highly efficient blue phosphorescence was thus attained with good OLED performance using **2a** and **3a**. In comparison with the CF_3-substituted complex **1** (scheme 1) showing significantly blue-shifted photoluminescence at 458 nm, phosphorescence for **2a** and **3a** was observed at a maximum wavelength (λ_{max}) of 495 and 494 nm, respectively. The exceedingly lower Φ_{PL} (~1%) for complex **1**, in comparison with the Φ_{PL} values for **2a** (24%) and **3a** (18%) in CH_2Cl_2 solution, was rationalized by the stabilized metal centered d-d* triplet state (^{3}MC d-d*) relatively to its ^{3}MLCT π-π*, the reverse ordering being found for **2a** and **3a.**

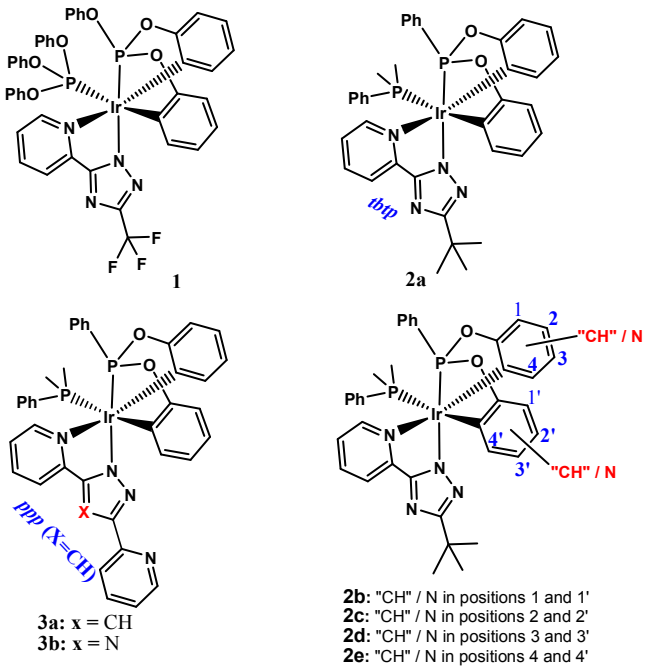

Scheme 1. Chemical structures of the relevant Ir complexes (*tbtp* and *ppp* refer to 2-(5-tert-butyl-2H-1,2,4-triazol-3-yl)pyridyl and 3-(3-(pyridin-2-yl)-1H-pyrazol-5-yl)pyridyl ligands, respectively).

Taking advantage of the fine-tunability of the electronic character, this work was undertaken to search for a strategy of improving the optical properties without altering the blue emission color. Preliminary quantum chemical calculations on complex **1** and a number of its homologous have shown that the electrons of the HOMO orbitals are mostly located on the phenoxide moieties of the P^C_2 ligand and Ir metal, while the highest electron density of the LUMO was located on the *tbtp* moiety (Scheme 1). [14] Whereas exceptionally good optical properties were reported for **2a** and **3a**, their electronic properties are still not yet completely investigated.

In the case of the mostly studied fluorescent material Alq_3 (tris-hydroxy-8, quinolinate aluminium, III), it is well known that an electron-withdrawing substituent on the *para*-position of the phenoxide ring depletes the HOMO (also found to be localized on the phenoxide side) electron density, lowering the energy level of the filled states. [16]

It was also reported that the substitution with an electron-

donating group on the *para*-position of the pyridine ring promotes the LUMO electron density (mostly located on this fragment) raising the energy level of the vacant states. In addition, both experimental [17] and theoretical investigations [18,19] have demonstrated the efficiency of the azasubstitution approach on the phenoxyl side of the quinolinate ligand in the tuning of the emission color of Alq_3. Assuming that this strategy can also hold for the complexes **2a** and **3a**, wider band gap and thus deep blue emitting analogues can be awaited. Exploring how the strategy can affect the photophysical properties of those complexes was the main objective of this work. In addition, we were interested in investigating the influence of the *tbtp/ppp* substitution (ongoing from complex **2a** to **3a**/**b**) on the electronic structure and a number of photophycal properties.As developed in the following sections, the azasubstitution on the phenoxide moieties of the $P^{\wedge}C_2$ ligand can constitute an efficient approach of tuning the energy gap between the ^{3}MLCT/π-π* and ^{3}MC/d-d* states, preserving the blue phosphorescence without fluorine substituent which is suspected to harm the device operational time.[11] We hope and are convinced that, the strategy reported herein, which, to the best of our knowledge, was not tried yet, should lead to improved physical properties of the investigated kind of organometalic compounds.

2. Computational methodology

Starting from the experimental X-ray structure, the ground-state geometry optimization of complex **1** was carried out at the density functional theory (DFT) using the M062X, [20] BP86 [21] and B3LYP [22] hybrid functionals, in combination with the 6-31G(d) basis set [23] for F, P, C, N, O, and H atoms and the "double-ζ" quality LANL2DZ basis set [24] for the Ir element. An effective core potential (ECP) replaces the inner core electrons of Ir, leaving the outer core $[(5s)^2(5p)^6]$ electrons and the $(5d)^6$ valence electrons of Ir(III). The molecular structures of the complexes in the singlet ground state (S_0), the lowest singlet (S_1) and triplet (T_1) excited states were fully optimized. Triplet states were calculated at the spin unrestricted UM062X level with a spin multiplicity of 3. The expected values calculated for $<S^2>$ were always smaller than 2.03. Solvent effects were considered within the SCRF (Self-Consistent Reaction Field) theory using the polarized continuum model (PCM) approach to model the interaction with the solvent. [25,26] The partial density of states (PDOS) spectra were created by convoluting the molecular orbital information with Gaussian curves of unit height and fwhm of 0.5 eV. All the calculations were done with the help of the B.01 revision of Gaussian 09 program package, [27] Gausssum 2.2.5 [28] being used for orbitals, PDOS and UV/Vis spectra analysis. The Molekel 4.3.2 user interface [29] was used to manipulate the structures and orbitals.

3. Results and discussion

3.1. Ground states properties

3.1.1. Molecular geometry

The MO62X, B3LYP and BP86 optimized ground (S_0) state geometrical parameters together with the X-ray crystal diffraction data [14] for the complex **1** (for the sake of comparison) are reported in Table 1. On one hand, despite the similar error levels in predicting the bond angles, the percent error (δ) indicates that the M062X functional provides a better accuracy (smaller δ) than both BP86 functional and the widely used hybrid B3LYP in the prediction of bond lengths, particularly the Ir-P_1, which was reported to play an important role in the physical properties of the class of complexes of interest. [14]

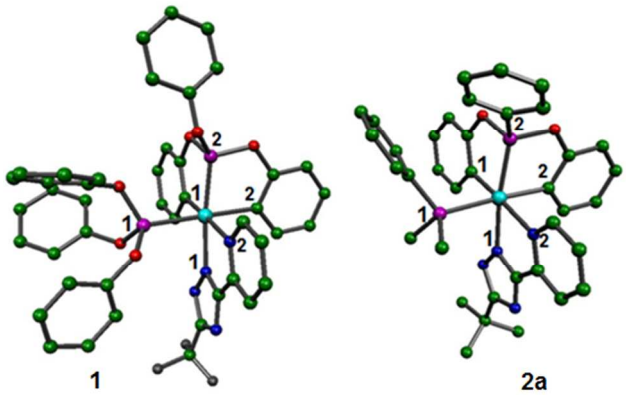

Fig.1. Optimized structures for **1** and **2a** in the S_0 state: Ir, P, N, O, C and F atoms are displayed in Blue-sky, Pink, Blue, Red, Green and Gray color (for clarity, Hydrogen atoms are not shown).

Table 1. Selected optimized parameters for complex **1** in the ground state: percent deviation (δ) versus XC functionals.

		M062X		B3LYP		BP86	
R & φ	Exp.[b]	Calc.[c]	δ [d]	Calc.[c]	δ [d]	Calc.[c]	δ [d]
		Bond length (R in Å)					
Ir-C_1	2.061(5)	2.043	-0.87	2.076	0.73	2.094	1.60
Ir-C_2	2.095(5)	2.068	-1.29	2.094	-0.05	2.077	-0.86
Ir-P_1	**2.269(15)**	**2.299**	**1.32**	**2.375**	**4.67**	**2.353**	**3.70**
Ir-P_2	2.171(14)	2.172	0.05	2.220	2.26	2.214	1.98
Ir-N_1	2.093(5)	2.136	2.05	2.117	1.15	2.109	0.76
Ir-N_2	2.145(5)	2.226	3.78	2.228	3.87	2.214	3.22
		Bond angle (φ in °)					
N_1-Ir-N_2		75.6		75.8		76.2	
C_1-Ir-C_2		91.7		90.0		89.9	
P_1-Ir-P_2		101.0		100.5		100.7	
N_1-Ir-P_2	171.9(14)	173.7	1.02	171.7	-0.11	171.5	-0.22
P_1-Ir-C_2		178.2		179.5		179.3	
C_1-Ir-N_2		176.3		175.8		175.6	

[a] The atom numbering scheme is given in Figure 1. [b] Crystal data (with the standard deviation in psrenthesis) from Ref. [14]. [c] Calculated. [d] $\delta(\%) = \frac{\text{calc} - \text{exp}}{\text{exp}} \times 100$

Table 2. Selected M062X optimized parameters for **2a**, **3a** and the aza-substituted derivatives in the ground state (S_0).

R & φ	**2a**	**2b**	**2c**	**2d**	**2e**	**3a**
			Bond length (R in Å)			
Ir-C_1	2.033	2.040	2.025	2.032	2.025	2.022
Ir-C_2	2.064	2.065	2.057	2.061	2.056	2.063
Ir-P_1	**2.379**	**2.375**	**2.381**	**2.378**	**2.382**	**2.383**
Ir-P_2	2.204	2.207	2.214	2.207	2.211	2.203
Ir-N_1	2.130	2.125	2.118	2.117	2.124	2.112
Ir-N_2	2.246	2.233	2.238	2.238	2.241	2.243
			Bond angle (φ in °)			
N_1-Ir-N_2	75.3	75.3	75.6	75.5	75.4	75.8
C_1-Ir-C_2	91.0	90.8	91.1	91.1	91.2	93.9
P_1-Ir-P_2	103.6	103.7	103.5	103.8	103.4	105.0
N_1-Ir-P_2	170.9	171.0	170.8	170.7	170.9	170.4
P_1-Ir-C_2	176.1	175.6	176.1	176.0	176.3	174.6
C_1-Ir-N_2	175.1	175.7	175.0	175.4	175.2	175.

***** The atom numbering scheme is given in Figure 1.

It becomes then clear that, from the geometrical structure viewpoint, the M062X/ECP-GEN-6-31G(d) level of theory is sufficient and reliable for Ir(III) complexes bearing phosphine ligand. This feature was recently reported by Wang et al.[30]

The table 2 gives the selected geometrical parameters for **2a**, **3a** and the derivatives under consideration as obtained using the M062X/ECP-GEN-6-31G(d) method. These results show that, on-going from **2a** to **3a**, none of the Ir-N, Ir-P and Ir-C bond lengths varies by more than 0.013Å. In comparison with complex **1** (Table 1) however, both the two Ir-P bonds are predicted to be lengthened by ~ 0.08 and 0.03 Å (respectively for Ir-P_1 and Ir-P_2) in **2a**, the Ir-N and Ir-C bond lengths remaining practically unchanged. The same observation can be made when comparing **1** to **3a** and to the aza-substitution derivatives (**2b-e**). Indeed, a careful analysis also shows that this heterosubstitution in the phenoxide moiety of the terdentate P^C_2 ligand in **2a** has only little influence on the metal-ligand bond (Ir-C, Ir-P and Ir-N) distances (less than 0.02 Å of change).

It is interesting to note that both the Ir-N and Ir-C bonds are shortened upon the aza-substitution, although this shortening does not exceed 0.011 Å for Ir-C (see Ir-C_1 in **2e**) and 0.018 Å for Ir-N (see Ir-N_1 in **2e**). The metal-ligand interaction can thus be expected to be enhanced to some extends. In the recent report by Lin et al., [14] it has been shown that the monodentate P-$(OPh)_3$(Ph = Phenyl ring) ligand in compound **1** and a number of other complexes (rendering the strongest Ir-P bonding) significantly destabilizes the ^{3}MC d-d state, such that its relative energy is higher than that of the (emitting) lowest-lying^3 MLCT/π-π* excited state.

Upon the weakening of the Ir-P bond, the energy gap between the ^{3}MLCT/π-π* and ^{3}MC/d-d* decreases. This could explain the highest emission quantum yield (Φ_{PL}) for P-$(OPh)_3$ bearing complexes *vs* $PPhMe_2$, PPh_2Me and PPh_3 based ones, whose Ir-P bond strength follows the order $P(OPh)_3$ > $PPhMe_2$ > PPh_2Me > PPh_3 (Me = Methyl). Interestingly, one may find that even the weakness of the Ir-P_1 bond strength from **1** to **2a** (Tables 1-2) is well predicted with M062X. Indeed, 2.299 and 2.379Å of bond length calculated for **1** and **2a** clearly show a stronger Ir-P_1 bond in compound **1**. From this point of view, the results summarized in Table 2 show no more than 0.004 Å of variation on the Ir-P_1 bond length, upon the aza-substitution of the two phenoxide moiety (scheme 1). We thus anticipate that none of the Ir-P_1 dependant photophysical properties (if any) may be affected by the envisaged aza-substitution.

3.1.2. Electronic properties

3.1.2.1. Molecular orbitals

The HOMO orbital for complex **1** has already been described on the basis of B3LYP calculations, to be of d(Ir) + π P^C_2) character, the LUMO being found to be of π* character, mainly localized the *tbtp* moity.[14] The contour plots of the frontier orbitals for a representative of the hetero-substitution derivatives (**2e**) is shown in Figure 2 (See Figure S1 for the remaining compounds, in the supporting material), the orbitals energies being listed in Table 3. For the sake of comparison, both complexes **1** and **2a** are also considered. For a better interpretation, the trends of the results discussed in this paragraph are plotted in Figure 3.

In complex **2a** and the derivatives **2b-e**, the LUMO shows the same bonding - antibonding pattern: it is localized on the *tbtp* ligand with the most significant contribution coming from the pyridyl side.

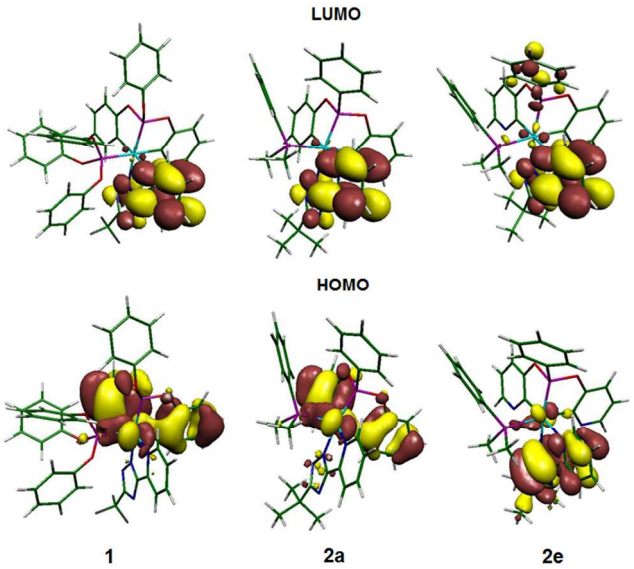

Fig.2. Contour plots of the highest occupied (HOMO) and lowest unoccupied (LUMO) molecular orbitals in gas phase for **1**, **2a** and **2e** as representative of the hetero-substitution derivatives (more details are provided by Figure S1 in the ESI).

Table 3. Frontier molecular orbitals (ε_{HOMO} and ε_{LUMO}) computed at two different levels of theory.

Cplx*	M062X		BP86	
	ε_{HOMO}	ε_{LUMO}	ε_{HOMO}	ε_{LUMO}
1	-7.15	-0.70	-5.14	-2.40
2a	-6.75	-0.56	-4.60	-2.21
2b	-7.04	-0.71	-4.88	-2.36
2c	-7.25	-0.80	-5.09	-2.45
2d	-7.07	-0.72	-4.85	-2.37
2e	-6.65	-0.40	-4.64	-2.06
3a	-6.60	-0.47	-4.49	-2.14
3b	-6.72	-0.61	-4.60	-2.28

* Cplx = Complex. Values are given in eV.

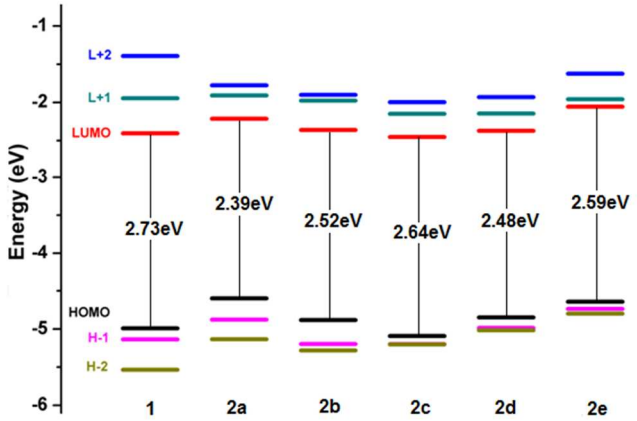

Fig.3. Evolution of MO energies for the three highest occupied (HOMOs) and three lowest unoccupied (LUMOs) orbitals as obtained using BP86 method (for comparison, FMO energies of complex **1** are also shown).

The same character was also reported for **1**.[14] In comparison with the molecule parent (**2a**), a relatively significant difference is however observed for the HOMO electron density distribution, which is attributed to the aza-substitution. While being localized on the phenoxyl moieties of the terdentate P^C_2 ligand, with some fairly significant contribution from Ir d orbitals in **2a** and **1**, the HOMO is mostly localized on the *tbtp* ligand in **2c** and **2e** with an admixture of Ir d character.

For **2d** and **2b** derivatives, the HOMO is still mainly localized on the phenoxyl sides, but with a mixture of π character from the triazolyl side of the *tbtp* ligand and some d chatacterfrom Ir. Such an electronic structural change can be traced back to the geometrical Ir - *tbtp* interaction induced by the Ir-N bond shortening upon the aza-substitution, which itself can be interpreted as a consequence of charge redistribution. In comparison with **2a**, a deep analysis of both the frontier orbitals (Figures 2 and S1) and the PDOS (Figure S2 in the ESI) for **3a** reveals an important change on the HOMO electron density, which is no longer exclusively made of contributions from the two phenoxide moities of the P^C_2 ligand up on *tbtp*/*ppp* substitution.

From the orbital energy values presented in Table 3, one can find that the magnitude of the eigenvalues and their relative differences are sensitive to the calculation approach used. The BP86 computed HOMO-LUMO energy gap (Eg) for **1**, **2a** and **3a**, ranging from 2.35 to 2.79 eV (Fig. 3), is however found to be in a very excellent agreement with experimental data reported for other blue phosphorescent materials.[31] It is particularly interesting to note how well the relative trend of the values is supported by the two sets of values. A general feature derived from both M062X and BP86 series of results is that the aza-substitution on positions 1-1', 2-2', 3-3' and 4-4' (scheme 1) stabilizes both the HOMO and LUMO, except for the LUMO, which is destabilized by the aza-substitution on positions 4-4'.The resulting net effect appears to be a slightly increasing Eg, depending on the position of the aza-substitution. The largest increase, with the respect to **2a** was predicted for **2c**, followed by **2e** and **2b** (respectively). Ongoing from compound **2a** to **1**, about 0.26 eV (and 0.34 eV) of increase is revealed by both BP86 and M062X. This is in a very good agreement with the experimental blue shifted emission spectra reported by H.-C Lin et al. [14] According to the same report, an enhanced performance for **2a** and **3a** (comparatively to **1** and some complexes bearing phenoxyl groups non linked to the metal atom) arises from a better matching of energy levels between dopant and electron/hole transporting materials upon replacing phenoxyl with phenyl fragment (scheme 1), and the introduction of additional electron conducting pyridyl fragment for **3a**. From this viewpoint, it becomes clear that the aza-substitution under investigation can provide a powerful way of tuning the energy levels between dopant and electron/hole transporting materials, preserving the blue phosphorescence, which, considering the slightly increased LUMO-HOMO gap, is anticipated to be shifted to the deep blue.

Table 4. Ionization potentials (IP), electron affinities (EA), extraction potentials for hole (HEP) and electron (EEP), and inner reorganization energies for electron/hole (λ_e/λ_h) for the studied molecules.

Cplx*	IP(v)	EA(v)	IP(a)	EA(a)	HEP	EEP	λ_h	λ_e
2a	6.31	0.46	6.19	0.60	5.89	0.70	0.42	0.24
2b	6.58	0.61	6.46	0.75	6.15	0.86	0.43	0.25
2c	6.76	0.73	6.75	0.86	6.36	0.97	0.39	0.24
2d	6.53	0.68	6.46	0.80	6.14	0.91	0.40	0.23
2e	6.33	0.44	6.25	0.53	5.93	0.67	0.39	0.23
3a	6.12	0.45	6.03	0.59	5.72	0.70	0.39	0.25
3b	6.23	0.58	6.14	0.74	5.85	0.83	0.38	0.26

*Cplx = Complex. (v) and (a) indicate vertical and adiabatic values, respectively. BP86 values are in eV.

3.1.2.2. Ionization potentials (IPs), electron affinities (EAs), extraction potentials for hole (HEP) and electron (EEP), and inner reorganization energies for electron (λ_e)/hole (λ_h)

Electron affinity (EA), ionization potential (IP), and charge mobility are other key factors in the design of optoelectronic materials. Indeed, the charge injection properties of luminescent materials can be evaluated by the EA and IP, which are also closely relative to the LUMO and HOMO, respectively. [32] A large EA (small IP) suggests the ease of electrons (holes) injection into the emitting materials from the electron (hole) transporting layer. The vertical IP (IP_v), adiabatic IP (IP_a), vertical EA (EA_v), and adiabatic EA (EA_a) for the studied complexes are listed in Table 4. Here, one can find that the smallest IP and EA values were predicted for **3a**. In comparison with **2a**, the EA and IP values for **2e** were predicted to be of the same magnitude: 6.33 eV (6.25 eV) *vs* 6.31 eV (6.19 eV) of IP_v (IP_a) and 0.44 eV (0.53 eV) *vs* 0.46 eV (0.60 eV) of EA_v (EA_a).

The inner reorganization energies λ_e and λ_h also shown in Table 4 were calculated using equations (1) and (2). In the equation (1), HEP represents the hole extraction potential, which

is the energy difference between neutral molecule (M) and cationic form (M^+), using M^+ geometry. In the equation (2), EEP is the electron extraction potential, which is the energy difference between M and M^- (anionic), using M^- geometry.

$$\lambda_h = IP_V - HEP \quad (1)$$

$$\lambda_e = EEP - EA_V \quad (2)$$

The results indicate that both the recently characterized blue phosphorescent **3a** and **2a** are electron transporters ($\lambda_e < \lambda_h$), with comparable λ_e (0.24 *vs* 0.25eV, respectively). The results also suggest that the differences between λ_h and λ_e for **2a** and **2b-e** are not very significant, implying that a better or comparable charge transport rate can be awaited from the aza-substitution derivatives. In some cases (**2c**, **2d** and **2e**), both λ_h and λ_e are smaller than those for the blue phosphorescent **2a**. From this viewpoint, one may conclude that the aza-substitution in positions 2-2', 3-3' and 4-4' (scheme 1) of complex **2a**, can improve its charge transporting property.

Table 5. Selected DFT-M062X bond lengths (R) in the three investigated states (S_0, ^{3}MLCT, and ^{3}MC) for **1** and **2a**.*

	1			2a		
R (in Å)	S_0	^{3}MLCT	^{3}MC	S_0	^{3}MLCT	^{3}MC
Ir-C_1	2.043	2.050	1.978	2.033	2.038	1.977
Ir-C_2	2.068	2.065	2.005	2.064	2.062	2.013
Ir-P_1	2.299	2.306	2.432	2.379	2.389	2.480
Ir-P_2	2.172	2.171	2.431	2.204	2.203	2.416
Ir-N_1	2.136	2.131	2.338	2.130	2.120	2.350
Ir-N_2	2.226	2.195	2.275	2.246	2.208	2.283
$E_{tot.}$ §	0	77.71	73.20	0	71.46	71.83

* The atom numbering scheme is shown in Figure 1. §Total energy relative to the ground state

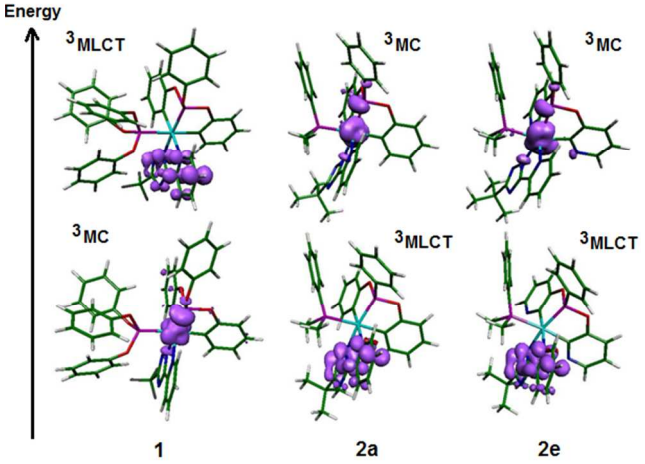

Fig.4. Computed spin density distribution (isocontour value of 5.10^{-3} au) for **1**, **2a** and **2e** in both the optimized ^{3}MLCT and ^{3}MC structures.

These results (based on BP86) are in good qualitative agreement with those based on M062X (see Table S1 in the ESI), and this consistency gives credit to the conclusions (at least qualitative) derived from them.

3.2. Excited states properties

In order to get more insights in the drastic difference between the observed optical properties of **1** and **2a** (**3a**), additional DFT and TD-DFT calculations were performed on these two complexes. In addition to the ground-state (S_0) geometries described above (section 3.1), a full structural optimization of the lowest ^{3}MLCT and ^{3}MC states for both **1** and **2a** was performed at the unrestricted level of theory. The lowest ^{3}MLCT states of the two complexes were found by performing an unrestricted T_1 optimization, starting from the optimized S_0 geometry. To locate the ^{3}MC, the structures were distorted in order to get a good starting guess for a subsequent unrestricted triplet optimization. This simple philosophy has been described and successfully used elsewhere. [14,33] The major geometrical changes are summarized in Table 5. For both systems, the distortion of the geometry from the S_0 to the ^{3}MLCT state is small. The Ir-C_2, Ir-P_2 and Ir-N_1 bonds for the triplet are slightly shorter than those in the S_0 state, while a relatively large shortening (by ~0.038 Å) is predicted for Ir-N_2. The Ir-C_1 and Ir-P_1bonds are only slightly lengthened. On the other hand, the geometric displacements from the S_0 to the ^{3}MC state are relatively large and the same bonds vary by 0.05–0.22 Å in the ^{3}MC state.

The spin densities calculated for the ^{3}MC states as shown in Figure 4, reflect the σ-interactions that characterize these states and corroborate their metal-centered character. For comparison, the spin density for **2e** as representative of the derivatives under study is also displayed (see Figure S3 for **2b-d**). From this aspect, the same behavior found for **2a** and **2b-e** implies that the aza-substitution does not change the character of the ^{3}MLCT and ^{3}MC states. More relevant than the molecular structure is the relative energy position of the ^{3}MC states, with respect to the emitting triplet state (^{3}MLCT). The relation between the structure and energetics for the S_0 and the two triplet states (^{3}MLCT and ^{3}MC) of complexes **1** and **2a** is illustrated by the calculated energy diagram in Figure 5, with the influence of the aza-substitution on the structure-energy relationship being also shown.

3.3. Photophysical properties

The radiative (k_r) and non-radiative (k_{nr}) rate constants are linked to the phosphorescence quantum yield (Φ_{PL}) from an emissive excited state to the ground state to by the equation (3):

$$\Phi_{PL} = k_r / (k_r + k_{nr}) \quad (3)$$

Theoretically, k_r is related to the mixing between S_1 and T_1, which is proportional to the Spin-Orbit Coupling (SOC) and inversely proportional to the energy difference between the two states, according to equation (4):

$$k_r = \gamma \frac{\langle \Psi_{S1} | H_{S0} | \Psi_{S0} \rangle^2 . \mu_{S1}^2}{(\Delta E_{S1\text{-}T1})^2}, \text{ with } \gamma = \frac{16\pi^2 10^6 n^3 E_{em}^3}{3 h \varepsilon_0} \quad (4)$$

Here, μ_{S1} is the transition electric dipole moment in $S_0 \rightarrow S_1$ transition, E_{em} represents the emission energy in cm^{-1} while n, h, and ε_0 are (respectively) the refractive index, the Planck's constant and the permittivity in vacuum.

As shown in many reports by Yersin et al., [34] the total zero field splitting (ZFS) is an information that carries an important message, since its value displays the extent of MLCT perturbation in the emitting T_1 state. Indeed, significant splitting of a triplet state is only present if the SOC induced by the heavy metal atom ion (Ir) is effective, and provides mixing of the triplet substates with higher lying triplets and singlets. Such a mixture is particularly responsible for an increase of k_r and the reduction of the emission decay time.

Using equation (4), we recently provided a valuable theoretical analysis of the evolution of Φ_{PL} within a series of compounds, [35] with the aid of computed Δ_{ES1-T1}, μ_{S1} and ZFS. It was demonstrated that the geometrical isomerism and the twisting degree of the ligand have a great influence on the ISC rate. The same parameters have been computed for the complexes **1**, **2a-e** and **3a-b**: the results are listed in Table 6. From the analysis of these values, none of the evaluated parameters could explain the drastically low Φ_{PL} observed for **1** (1%) *versus* those for **2a** (24%) and **3a** (18%). Indeed, on-going from **2a** to **1** (and **3a**), no more than 0.07 of difference was found on the ZFS values, implying that the SOC is not likely to affect the observed Φ_{PL}.

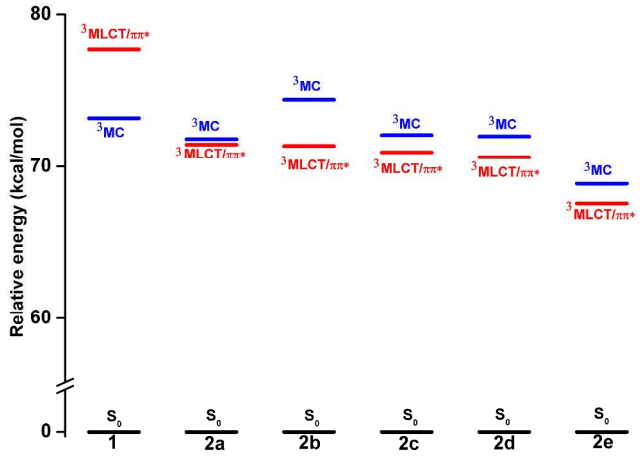

Fig.5. ^{3}MLCT/π-π* and ^{3}MC/d-d* energy levels for **2a** and the derivatives **2b-e** (for comparison, complex **1** is also considered).

Table 6. The singlet-triplet splitting energy (ΔE_{S1-T1} in eV), transition electric dipole moment (μ_{S1} in Debye), and Zero-Field Splitting (ZFS) for the complexes investigated (**1**, **2a-e** and **3a-b**).

Cplx*	E_{S1}	E_{T1}	ΔE_{S1-T1}	μ^2_{S1}	ZFS [a]
1	3.921	2.654	1.267	2.240	0.03
2a	3.665	2.492	1.173	1.989	0.00
2b	3.673	2.488	1.185	1.536	0.15
2c	3.668	2.486	1.182	1.673	0.16
2d	3.656	2.489	1.167	1.397	0.16
2e	3.571	2.455	1.116	1.656	0.15
3a	3.678	2.634	1.044	3.910	0.07
3b	2.192	1.901	0.291	3.803	0.06

* Cplx = Complex. Unless otherwise stated, the results were computed at TD-M062X. [a] Computed with the aid of UPB86 at the T_1 optimized geometries (the values are given relative to the ZFS of **2a**).

Table 7. Phosphorescence ($\lambda_{ph.}$ in nm) wavelengths and excitation orbitals (EO).

	B3LYP		M062X		Exp. [a]	
Cplx*	λ_{ph}	Assignment [b]	λ_{ph}	Assignment [b]	Φ_{PL}	$\lambda_{ph.}$
1	524	H-1→L(42%)+H→L(30%)	467	H→L (82%)	0.01	458
2a	561	H→L(53%) + H-1→L(39%)	497	H→L (85%)	0.24	495
2b			498	H→L (91%)		
2c			498	H→L (93%)		
2d			498	H→L (91%)		
2e			505	H→L (74%)		

*Cplx = Complex. [a] Experimental data from Ref. [14]. [b] H = HOMO, L = LUMO.

In addition, the smallest Δ_{ES1-T1} (1.04 eV) and largest μ_{S1} (3.91 D) for **3a** could be expected to lead to the highest Φ_{PL} among the three complexes. However, the experimental results do not show this. Although not stated in the report by Lin and his co-workers, [14] the small Φ_{PL} of **3a** (18%) compared to the one for **2a** (24%) can be thought to be due to the substituting pyridyl group. Indeed, the torsional degree of freedom of phenyl is suspected to induce a competing nonradioactive channel, mainly determining the low emission efficiency observed for some Ir (III) complexes). [36] In the studied complexes however, the ^{3}MLCT/π-π* and ^{3}MC/d-d* energy splitting seems to be the most suitable parameter to explain the reported differences in the optical properties.

According to our computational results, the ^{3}MC lies below the ^{3}MLCT in complex **1**, while located above the ^{3}MLCT in the case of **2a** and its aza-substitution derivatives considered herein. This result is in total (qualitative) agreement with the reported finding by Lin et al., [14] which, based on B3LYP calculation, was used to explain the extremely low Φ_{PL} observed for **1**. Indeed, the radiationless ^{3}MLCT/π-π*→^{3}MC/d-d* pathway is expected to be efficient in this case, [37] accounting for its higher k_{nr} value (4.09×10^6 *vs* 2.68×10^5 for **2a**), that is, the lowest Φ_{PL} (1.2% *vs* 24% for **2a**) and shortest observed lifetime (244 ns *vs* 5.88 µs for **2a**). [14] According to the results summarized in Figure 5, more enhanced physical properties (smaller k_{nr}, higher Φ_{PL}, and longest lifetime) can be awaited for the derivatives **2b-e** (with respect to those observed for **2a** and thus for **3a**), due to their larger ^{3}MLCT/π-π* and ^{3}MC/d-d* energy splitting.

From the emission energies, the transition nature, and available experimental values listed in Table 7, one may find that M062X performs better than the B3LYP used in the report by Lin et al. [14] Indeed, the M062X emission energies for **1** (2.65 eV / 467 nm) and **2a** (2.49 eV / 497 nm) are in excellent agreement with experimental values (i.e 458 and 495 nm [14]), those based on B3LYP (524 and 561 nm) being found to vary by 64 and 66 nm from the experimental data. On the basis of the results reported herein, it can be found that the emission energy of complex **2a** is quite similar to that of complexes **2b-d** (~2.49 eV / 498 nm). All these new complexes were predicted to have almost the same phosphorescence characters, that is, a mixture of MLCT and ILCT.

Conclusion

With the aid of electronic structure methods based on DFT (M062X and BP86) and TD-M062X, the influence of the aza-

substitution on the geometrical, electronic and a number of optoelectronic properties of the newly reported blue phosphorescent **2a**, bearing dicyclometalated phosphite tripod ligand ($P^{\wedge}C_2$) was investigated. The aza-substitution on the phenoxide side of the $P^{\wedge}C_2$ ligand was found to stabilize both the HOMO and LUMO, the net effect being a slight increase in the LUMO-HOMO energy gap. The Ir-P bond length recently shown to play an important role on the photophysical properties of this family of complexes was found to be preserved, only a minor change in the SOC being predicted. More interestingly, the aza-substitution was found to destabilize the non-radiative ^{3}MC/d-d* excited states, enhancing the energy separation from the radiative ^{3}MLCT/π-π* state, without altering the blue phosphorescence. All these features make these aza-substitution derivatives **2b-e** potential candidates as deep blue phosphorescent.

Acknowledgements

The authors thank the National Natural Science Foundation of China for financial support (Grant Nos. 21221061, 21273219). Dr G. GAHUNGU thanks the financial supports by TWAS-CAS Fellowship and the Chinese Ministry of Sciences and Technology (MOST) for the equipment Donation.

Notes and references

[a] *Changchun Institute of Applied Chemistry, Chinese Academy of Science, Key Laboratory of Rare Earth Utilization, 130022, Changchun, China. Fax: +86-431-85698041; Tel: +86-431-85262801; E-mail: zjwu@ciac.jl.cn*

[b] *Université du Burundi, Faculté des Sciences, Département de Chimie, BP.2700, Bujumbura - Burundi. Fax:* (+257)-22223288. *Tel: (+257)-79055192; E-mail:godefroid.gahungu@ub.edu.bi.*

†Electronic Supplementary Information (ESI) available: xyz coordinates for the optimized structures of complexes **1**, **2a-e** and **3a-b** in both the S_0 and T_1 states. Figure S_1 for contour plots of the highest occupied (HOMO) and lowest unoccupied (LUMO) molecular orbitals in gas phase. Figure S2 for Partial Density of State (PDOS) of complexes **2a** and **3a**. Figure S3 for the computed spin density distribution in **2b-d** in both the ^{3}MLCT and ^{3}MC structures. Table S1 lists the ionization potentials, electron affinities, extraction potentials for hole and electron, and inner reorganization energies for electron based M062X.

1 C. Adachi, M. A. Baldo, M. E. Thompson and S. R. Forrest, *J. Appl. Phys.*, 2001, **90**, 5048.
2 M. A. Baldo, S. Lamansky, P. E. Burrows, M. E. Thompson and S. R. Forrest, *Appl. Phys. Lett.*, 1999, **75**, 4.
3 A. Tsuboyama, H. Iwawaki, M. Furugori, T. Mukaide, J. Kamatani, S. Igawa, T. Moriyama, S. Miura, T. Takiguchi, S. Okada, M. Hoshino and K. Ueno, *J. Am. Chem. Soc.*, 2003, **125**, 12971.
4 J. Y. Shen, C. Y. Lee, T.-H. Huang, J. T. Lin, Y.-T. Tao, C.-H. Chien and C. J. Tsai, *Mater. Chem.*, 2005, **15**, 2455.
5 S. O. Kim, K. H. Lee, G. Y. Kim, J. H. Seo, Y. K. Kim and S. S. Yoon, *Synth. Metals.*, 2010, **160**, 1259.
6 C. Adachi, R. C. Kwong, P. Djurovich, V. Adamovich, M. A. Baldo, M. E. Thompson and S. R. Forrest, *Appl. Phys. Lett.*, 2001, **79**, 2082.
7 R. J. Holmes, S. R. Forrest, Y. J. Tung, R. C. Kwong, J. J. Brown, S. Garon and M. E. Thompson, *Appl. Phys. Lett.*, 2003, **82**, 2422.
8 S. Tokito, T. Iijima, Y. Suzuri, H. Kita, T. Tsuzuki and F. Sato, *Appl. Phys. Lett.*, 2003, **83**, 569.
9 T. Sajoto, A. B. Tamayo, P. I. Djurovich, M. Yousufuddin, R. Bau, M. E. Thompson, R. J. Holmes and S. R. Forrest. Abstracts of Papers of the American Chemical Society, 2005, **229**, U1031.
10 J. Li, P. I. Djurovich, B. D. Alleyne, M. Yousufuddin, N. N. Ho, J. C. Thomas, J. C. Peters, R. Bau and M. E. Thompson. *Inorg. Chem.*, 2005, **44**, 1713.
11 S. Haneder, E. Da Como, J. Feldmann, J. M. Lupton, C. Lennartz, P. Erk, E. Fuchs, O. Molt, I. Muenster, C. Schildknecht and G. Wagenblast, *Adv. Mater.*,2008, **20**, 3325.
12 S.-C. Lo, C. P. Shipley, R. N. Bera, R. E. Harding, A. R. Cowley, P. L. Burn and I. D. W. Samuel, *Chem. Mater.*, 2006, **18**, 5119.
13 S. J. Lee, K.-M. Park, K. Yang and Y. Kang, *Inorg. Chem.*, 2009, **48**, 1030.
14 C.-H. Lin, Y.-Y. Chang, J.-Y. Hung, C.-Y. Lin, Y. Chi, M.-W. Chung, C.-L. Lin, P.-T. Chou, G.-H. Lee, C.-H. Chang and W.-C. Lin. *Angew. Chem. Int. Ed.*, 2011, **123**, 3240.
15 (a) Y.-C. Chiu, C.-H. Lin, J.-Y. Hung, Y. Chi, Y.-M. Cheng, K.-W. Wang, M.-W. Chung, G.-H. Lee and P.-T. Chou, *Inorg. Chem.*, 2009, **48**, 8164; (b) J.-Y. Hung, C.-H. Lin, Y. Chi, M.-W. Chung, Y.-J. Chen, G.-H. Lee, P.-T. Chou, C.-C. Chen and C.-C. Wu, *J. Mater. Chem.*, 2010, **20**, 7682.
16 (a) S. A. Van Slyke, P. S. Brynn and F. V.Levecchio, U.S. Patent Nº.5150006, 1992. (b) P. E. Burrow, Z. Shen, V. Bulvoic, D. M. McCarty, S. R. Forrest, J. A. Cronin and M. E.Thompson, *J. Appl. Phys.*, 1996, **79**, 7991. (c) M. Sugimoto, M. Anzai, K. Sakanoue and S. Sakaki, *Appl. Phys. Lett.*, 2001, **79**, 2348.
17 S.-H Liao, J.-R Shiu, S.-W Liu, S.-J Yeh, Y.-H. Chen, C.-Ti Chen, T.-J. Chow and C.-I. Wu, *J. Am. Chem. Soc.*, 2008, **131**, 763.
18 G. Gahungu and J.-P Zhang, *J. Phys. Chem. B*, 2005, **109**, 17762.
19 G. Gahungu, J. P. Zhang, V. Ntakarutimana and N. Gahungu, *J. Phys. Chem. A,* 2010, **114**, 652.
20 Y. Zhao and D. Truhlar, *Theor. Chem. Acc.*,2008, **120**, 215.
21 J. P. Perdew, *Phys. Rev. B* 1986, **33**, 8822.
22 (a) A. D. Becke, J. *Chem. Phys*., 1993, **98**, 5648. (b) C. T. Lee, W. T. Yang, R. G. Parr, *Phys Rev B* 1988, **37**, 785. (c) A. D. Becke, *Phys Rev A* 1988, **38**, 3098.
23 (a) M. M. Francl, W. J. Pietro, W. J. Hehre, J. S. Binkley, M. S. Gordon,; D. J. Defrees and J. A. Pople, *J. Chem. Phys.*, 1982, **77**, 3654. (b) M. S. Gordon, *Chem. Phys. Lett*., 1980, **76**, 163. (c) P. C. Hariharan and J. A. Pople, *Mol. Phys.*, 1974, **27**, 209. (d) M. J. Frisch, J., A. Pople and J. S. Binkley, *J. Chem. Phys.,* 1984, **80**, 3265.
24 P. J. Hay and W. R. Wadt, *J. Chem. Phys.*, 1985, **82**, 299.
25 C. S. Cramer and D. G. Truhlar, *Solvent Effects & Chemical Reactivity*; Kluwer: Dordrecht, The Netherlands, 1996.
26 J. Tomasi and M. Persico, *Chem. Rev.*, 1994, **94**, 2027.
27 M. J. Frisch, G. W. Trucks, H. B. Schlegel, G. E. Scuseria, M. A. Robb, J. R. Cheeseman, G. Scalmani, V. Barone, B. Mennucci, G. A. Petersson, H. Nakatsuji, M. Caricato, X. Li, H. P. Hratchian, A. F Izmaylov, J. Bloino, G. Zheng, J. L Sonnenberg, M. Hada, M. Ehara, K. Toyota, R. Fukuda, J. Hasegawa, M. Ishida, T. Nakajima, Y. Honda, O. Kitao, H. Nakai, T. Vreven, Jr., J. A Montgomery, J. E Peralta, F. Ogliaro, M. Bearpark, J. J. Heyd, E. Brothers, K. N. Kudin, V. N. Staroverov, T. Keith, R. Kobayashi, J. Normand, K. Raghavachari, A. Rendell, J. C. Burant, S. S. Iyengar, J. Tomasi, M. Cossi, N. Rega, J. M. Millam, M. Klene, J. E Knox, J. B. Cross, V. Bakken, C. Adamo, J. Jaramillo, R. Gomperts, R. E Stratmann, O. Yazyev, A. J. Austin, R. Cammi, C. Pomelli, J. W. Ochterski, R. L. Martin, K. Morokuma, V. G. Zakrzewski, G. A. Voth, P. Salvador, J. J. Dannenberg, S. Dapprich, A. D Daniels, O. Farkas, J. B. Foresman, J. V. Ortiz, J. Cioslowski & D. J. Fox, Gaussian 09, Revision B.01. Gaussian, Inc., Wallingford CT, 2010.
28 N. M. O'Boyle, A. L. Tenderholt and K. M. Langner, *J. Comput. Chem.*, 2008, **29**, 839.
29 U. Varetto, MOLEKEL Version; Swiss National Supercomputing Centre: Lugano (Switzerland).
30 J. Wang, F.-Q Bai, B.-H Xia and H.-X Zhang, *J. Phys. Chem. A*, 2011, **115**, 11689.
31 L. Chen, H. You, C. Yang, D. Ma and J. Qin, *Chem. Commun.*, 2007, **13**, 1352.

32 L. L. Shi, Y. Liao, G. C. Yang, Z. M. Su and S. S. Zhao, *Inorg. Chem.*, 2008, **47**, 2347.
33 M. Abrahamsson, M. J. Lundqvist, H. Wolpher, O. Johansson, L. Eriksson, J. Bergquist, T. Rasmussen, H.-C. Becker, L. Hammarstrom, P.-O. Norrby, B. Akermark and P. Persson, *Inorg. Chem.*, 2008, **47**, 3540.
34 (a) H. Yersin, W. Humbs and J. Strasser, *Coord. Chem. Rev.*, 1997, **159**, 325; (b) H. Yersin and J. Strasser, *J. Lumin.*, 1997, **72–74**, 462; (c) H. Yersin, W. Humbs and J. Strasser, *Top. Curr. Chem.*, 1997, **191**, 153.
35 (a) G. Gahungu, , J.-J. Su, Y.-Q. Liu, X.-C. Qu, Y.-L. Si, X.-C. Shang and Z.-J. Wu, *J. Phys. Chem. C 2012*, **116**, 14575. (b) G. Gahungu, , J.-J. Su, Y.-Q. Liu, X.-C. Qu, Y.-L. Si, X.-C. Shang and Z.-J. Wu, 2012, *Dalton Trans*., 2012, 41, 10228.
36 S. Haneder, E. Da Como, J. Feldmann, J. M. Lupton, C. Lennartz, P. Erk, E. Fuchs, O. Molt, I. Münster, C. Schildknecht and G. Wagenblast, *Adv. Mater.*, 2008, **20**, 3325.
37 P.-T. Chou, Y. Chi, M.-W. Chung and C.-C. Lin, *Coord. Chem. Rev.*, 2011, **255**, 2653.